ELSEVIER

Biophysical Chemistry 105 (2003) 279–291

Biophysical Chemistry

www.elsevier.com/locate/bpc

The pH dependence of stability of the activation helix and the catalytic site of GART

Dimitrios Morikis[a,*], Adrian H. Elcock[b], Patricia A. Jennings[c], J. Andrew McCammon[c,d]

[a]*Department of Chemical and Environmental Engineering, University of California at Riverside, Riverside, CA 92521, USA*
[b]*Department of Biochemistry, University of Iowa, Iowa City, IA 52242, USA*
[c]*Department of Chemistry and Biochemistry, University of California at San Diego, La Jolla, CA 92093, USA*
[d]*Howard Hughes Medical Institute, and Department of Pharmacology, University of California at San Diego, La Jolla, CA 92093, USA*

Received 3 September 2002; accepted 1 November 2002

Abstract

We have predicted the free energy of unfolding for the pH-dependent helix-coil transition of the activation helix of GART using continuum electrostatic calculations and structural modeling. We have assigned the contributions of each element of secondary structure and of each ionizable residue, within and in the vicinity of the activation helix, to the stability of several fragments of GART that participate in the formation of the catalytic site. We demonstrate that the interaction of His121–His132 contributes 2.2 kcal/mol to the ionization free energy between pH 0 and approximately 6. We also show that the ionization state of a network of five histidines, His108, His119, His121, His132 and His137, and two aspartic acids Asp141 and Asp144, contributes approximately 12 kcal/mol to the stability of the catalytic site of GART, out of a total stability of 16 kcal/mol of the whole enzyme. These interactions are important for the formation of the catalytic site of GART.

Keywords: GART; Glycinamide ribonucleotide transformylase; Electrostatic calculations; Poisson–Boltzmann; pK_a; Stability; Helix–coil transition

1. Introduction

Glycinamide ribonucleotide transformylase (GART) is an enzyme that participates in the de novo purine biosynthetic pathway [1] and is a target for development of antineoplastic drugs [2–4]. GART undergoes a pH-dependent folding transition of an active site helix, which can regulate catalysis [3,5–8]. This helix–coil transition occurs at around neutral pH. At low pH GART possesses a 21-residue loop connecting strands β5 and β6, which is located on top of the catalytic site (Fig. 1). At high pH an 8-residue segment of this loop folds into a α-helix, and creates a hydrophobic environment for the catalytic site [7,8]. This loop-helix is termed the activation loop-helix. The schematic in Fig. 2 depicts the super-secondary

Abbreviations: GART, glycinamide ribonucleotide transformylase; PDB, Protein Data Bank; h–c, helix–coil; f–u, folded–unfolded.

*Corresponding author. Tel.: +1-909-787-2696; fax: +1-909-787-5696.

E-mail address: dmorikis@engr.ucr.edu (D. Morikis).

0301-4622/03/$ - see front matter © 2003 Elsevier Science B.V. All rights reserved.
doi:10.1016/S0301-4622(03)00079-6

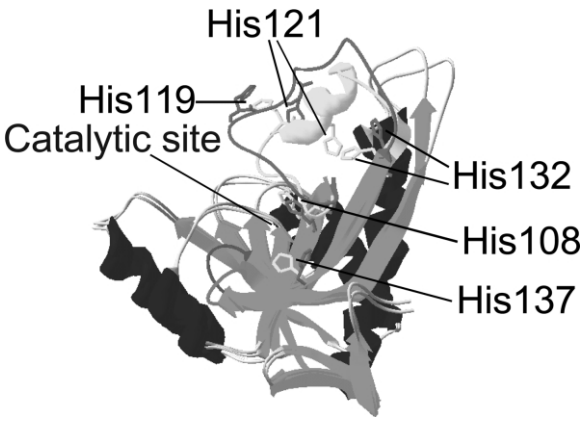

Fig. 1. Superposition of two GART structures at pH 3.5 and 7.5. Helices are drawn in blue, β-sheets are drawn in cyan, and loops are drawn in gray, with the exception of the activation loop-helix and the binding loop, which are drawn in yellow at high pH and in red at low pH, and the binding loop, which is drawn in green at high pH and in magenta at low pH. The five histidines involved in the formation of the catalytic site, His108, His119, His121, His132 and His137 are drawn in yellow and red at the high and low pH structures, respectively. The molecular models shown were prepared with the program Deep View/Swiss PDB Viewer [32].

structure and ionizable residues that participate in the formation of the catalytic site of GART at high pH. This part of GART includes strand β5-(activation loop-helix)-strand β6 and contains five histidines, His108 (in β5), His119 (in activation loop), His121 (in activation helix), and His132 and His137 (in β6) (Figs. 1 and 2). We have proposed that His121 act a molecular switch for the helix formation, while strongly interacting with His132 [8]. We have also shown that His119 plays a role, likely secondary, in the stability of the activation helix [8] and that the highly conserved catalytic site residues His108 and His137 are in strong electrostatic coupling at high pH [9]. In addition, when substrate is bound, residue Asp144 of the flexible loop sequentially attached to β6 (Figs. 1 and 2), stabilizes the electrostatic microenvironment of the catalytic site, forming four-way interactions with His108, His137, and substrate GAR [9]. This latter loop termed the binding loop, changes orientation upon substrate binding.

In an effort to better understanding the contribution of the helix–coil transition in the formation of the catalytic site as a function of changes in solution pH, we have calculated electrostatic potentials using available crystallographic structures at high and low pH. The calculation of the electrostatic potentials is based on the solution of the linearized Poisson–Boltzmann equation using continuum solvent. We have used the electrostatic potentials to calculate ionization free energies, the charges, and apparent pK_a values for the ionizable residues of GART that participate in the pH-dependent helix–coil transition. Finally, we have used the mean net charges at each pH for the locally folded and locally unfolded structures of

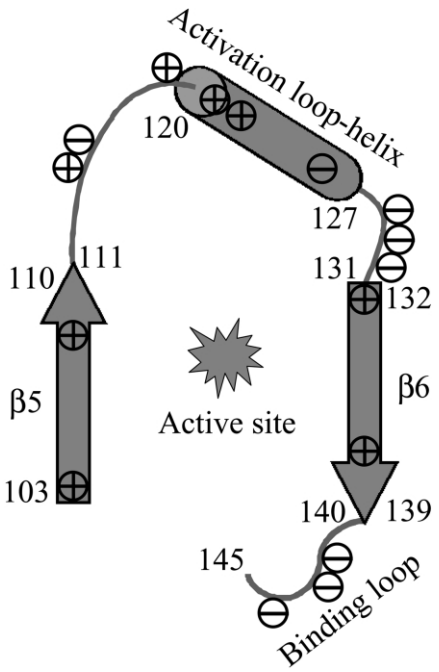

Fig. 2. A cartoon of the elements of secondary structure that form the catalytic site of the high pH GART structure. The figure depicts strand β5 (residues 103–110), activation loop/helix (residues 111–119 and 128–131 for loop and residues 120–127 for helix), strand β6 (residues 132–139), and binding loop (residues 140–145). Ionizable residues are marked in the figure, with negatively charged residues shown with a (−) symbol, positively charged residues shown with a (+) symbol. The numbers indicate the N-terminal and C-terminal of each element of secondary structure. Ionizable residues are: Arg103, His108, Lys114, Tyr115, His119, His121, Arg122, Glu126, Asp129, Glu130, Glu131, His132, His137, Asp141, Glu142, Asp144.

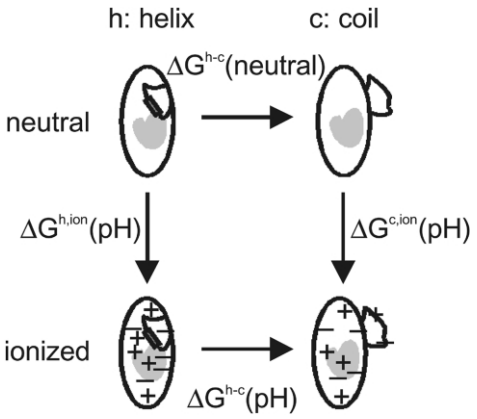

Fig. 3. The thermodynamic cycle of the helix-coil transition of the activation helix of GART. The shaded region corresponds to the catalytic site and the cylinder corresponds to the activation helix. The thermodynamic cycle decomposes the free energy of the helix–coil transition into a neutral and an ionized part. The bottom and the two vertical processes are pH-dependent and the top process is pH independent.

GART to calculate the ionization free energy of the helix–coil transition relative to a reference pH, $\Delta G^{h-c}(\mathrm{pH})$. In the locally folded structure of GART the activation helix is present, and in the locally unfolded structure of GART the activation helix is absent. The calculation of $\Delta G^{h-c}(\mathrm{pH})$ provides quantitative information on the relative stability of GART at high and low pHs. Local differences in the structures of the folded and unfolded states of the activation loop-helix and surrounding structure are responsible for differences in the charges, and the pK_a values associated with them, of individual ionizable residues. This methodology with its underlying assumptions is described elsewhere [10] and has been applied in the study of a number of systems [10–14].

2. Methodology

Fig. 3 outlines a thermodynamic cycle that provides a theoretical framework to describe the pH-dependent helix–coil transition of the activation helix of GART, following the formulation of Yang and Honig [10] and Vorobjev et al. [13]. The free energy of the helix–coil $(h-c)$ transition is split into two parts, a pH-independent and a pH-dependent part. The pH-independent part, $\Delta G^{h-c}(\mathrm{neutral})$, corresponds to free energy contributions that do not have titration-dependent origin, such as configurational entropy, hydrophobic interactions, desolvation of neutral polar groups, and hydrogen bond formation [10]. The pH-dependent part, $\Delta G^{h-c}(\mathrm{pH})$, corresponds to free energy contributions that include electrostatics. In each of the helical and coiled states ionization occurs with ionization free energies $\Delta G^{h,\mathrm{ion}}(\mathrm{pH})$ and $\Delta G^{c,\mathrm{ion}}(\mathrm{pH})$, respectively. The thermodynamic cycle is described by:

$$\Delta G^{h-c}(\mathrm{pH}) = \Delta G^{h-c}(\mathrm{neutral}) + \Delta G^{c,\mathrm{ion}}(\mathrm{pH}) - \Delta G^{h,\mathrm{ion}}(\mathrm{pH}) \quad (1)$$

or

$$\Delta G^{h-c}(\mathrm{pH}) = \Delta G^{h-c}(\mathrm{neutral}) + \Delta\Delta G^{c,h,\mathrm{ion}}(\mathrm{pH}) \quad (2)$$

The left term of Eq. (1) can be calculated using Tanford's equation that describes the pH dependence of protein stability for protein denaturation [15]:

$$\frac{\partial \Delta G^{f-u}(\mathrm{pH})}{\partial \mathrm{pH}} = 2.303RT(Q_{\mathrm{unfold}} - Q_{\mathrm{fold}}) \quad (3)$$

where ΔG^{f-u} is the free energy of unfolding, Q_{unfold} and Q_{fold}, are the proton charges of the unfolded and folded states, respectively, R is the gas constant, and T is the temperature. Tanford's equation can be re-written in the case of GART, where the absence or presence of the activation helix corresponds to a locally unfolded (c, coiled) or folded (h, helical) form, respectively. Then, integration yields

$$\Delta\Delta G^{h-c}(\mathrm{pH},\mathrm{pH}_1) = 2.303RT\int_{\mathrm{pH}_1}^{\mathrm{pH}} (\langle Q\rangle_c - \langle Q\rangle_h)\mathrm{dpH} \quad (4)$$

where

$$\Delta\Delta G^{h-c}(\mathrm{pH},\mathrm{pH}_1) = \Delta G^{h-c}(\mathrm{pH}) - \Delta G^{h-c}(\mathrm{pH}_1) \quad (5)$$

$\Delta G^{h-c}(\mathrm{pH})$ is the free energy of the helix-coil transition representing the stability of the activation helix, and $\langle Q\rangle_c$ and $\langle Q\rangle_h$ are the mean net charges of the protein in its coiled and helical states, respectively. Note that Eq. (5) corresponds to a difference of the free energy of the helix-coil transition from a reference value, $\Delta G^{h-c}(\mathrm{pH}_1)$. This reference value can be typically set at a pH, where most ionizable sites are fully neutral and fully charged (without fractional values) in both helical and coiled states, as suggested in Ref. [10]. In our case an appropriate value is $\mathrm{pH}_1=0$. This ensures that the mean net charges of the helical and coiled states at $\mathrm{pH}_1=0$ are about the same in Eq. (4), providing a constant ΔG^{h-c}. Combining (2) and (5) and taking into account that at pH_1

$$\Delta G^{h-c}(\mathrm{neutral})=\Delta G^{h-c}(\mathrm{pH}_1)-\Delta\Delta G^{c,h,ion}(\mathrm{pH}_1) \tag{6}$$

we get an expression that relates ΔG^{h-c} and the ionization free energy of unfolding in reference to pH_1

$$\Delta\Delta G^{h-c}(\mathrm{pH},\mathrm{pH}_1)=\Delta\Delta\Delta G^{c,h,ion}(\mathrm{pH},\mathrm{pH}_1) \tag{7}$$

where

$$\Delta\Delta\Delta G^{c,h,\mathrm{ion}}(\mathrm{pH},\mathrm{pH}_1)=\Delta\Delta G^{c,h,\mathrm{ion}}(\mathrm{pH})-\Delta\Delta G^{c,h,\mathrm{ion}}(\mathrm{pH}_1) \tag{8}$$

Yang and Honig [10] have shown that calculation of $\Delta\Delta G^{h-c}(\mathrm{pH},\mathrm{pH}_1)$ using the 'average charge method' of Eq. (4) and calculation of $\Delta\Delta\Delta G^{c,h,\mathrm{ion}}(\mathrm{pH},\mathrm{pH}_1)$ using a 'reduced site approximation method' yield nearly identical results after scaling at pH_1, which when compared to experimental data give an estimate for $\Delta G^{h-c}(\mathrm{neutral})$.

Here, we have used Eq. (4) to calculate differences of ionization free energies of unfolding $\Delta G^{h-c}(\mathrm{pH})$ (we will omit the free energy dependence on pH_1, hereafter, for simplicity of notation). The mean net charges, $\langle Q\rangle_c$ and $\langle Q\rangle_h$, as a function of pH were calculated from interactions of each ionizable site with all other ionizable sites in their ionized form using the multiple site titration clustering method [16] and pre-calculated intrinsic pK_a values [12,17], as described elsewhere [8]. Calculations were performed twice using structures with folded and unfolded GART activation helix. This methodology was implemented within the programs UHBD [18,19] and HYBRID [16], with the parameter set PARSE [20].

Two crystallographic structures of GART at high and low pH with the E70A mutation were used in the calculation. The E70A replacement results to a monomeric GART structure at low pH, allowing for a direct comparison to the monomeric GART structure at high pH [7]. The PDB codes are 3gar for the high pH structure and 2gar for the low pH structure [7]. The coordinates for the activation loop, residues 111–131, in the low pH GART structure (2gar) are missing because of lack of electron density, which is characteristic of the high flexibility of the activation loop at low pH. For our calculations we have generated the coordinates of the activation loop of GART of the low pH structure by (1) superimposing the coordinates of the high and low pH GART structures using the C_α atoms outside the activation loop, (2) transferring the coordinates of the activation loop of the high pH structure to the low pH structure, (3) locally minimizing the coordinates of the boundary residues of the activation loop and the rest of the protein, residues Ser110, Leu111, Glu131, His132, (4) unfolding the transferred coordinates in the low pH structure, using the method of Elcock [14]. The unfolding method of Elcock utilizes molecular mechanics to apply a step-wise explosion of the folded coordinate structure, which results in native-like unfolded structure in terms of shape, but with a small number of the original non-bonded contacts and increased solvent accessibility. This was achieved iteratively by increasing the minimum distance of van der Waals interactions, described by the 12-6 Lennard–Jones potentials, in the CHARMM22 force field [21], followed by 50 steps of steepest descent and 250 steps of conjugate gradient energy minimization using CHARMM [22]. Six iterations were used with increments for the minimum distance of van der Waals interactions of 1 Å per iteration up to 6 Å. At the end of the procedure two rounds of local minimization were performed on the unfolded

coordinates with normal minimum van der Waals distances to remove the strain on bond lengths and other covalent geometry parameters, induced by the explosion procedure. Electrostatic interactions were not included in any of the molecular mechanics simulations for the explosion of the activation helix coordinates. Elcock has shown that this unfolding method produces results in closer agreement with experimental data compared to modeled extended unfolded structures (e.g. with $\phi = \psi = 180^{o}$ dihedral angles) in similar studies of protein stability that require modeling of the unfolded states [14].

In preparation for our calculations, the program WHAT IF (version 99; [23,24]) was used first to add hydrogen atoms in the crystallographic coordinates, and second to perform a global hydrogen bonding network optimization [23,25]. The second step was deemed necessary prior to the electrostatic calculations to correct the side chain orientation of histidines, asparagines and glutamines and to discriminate the initial hydrogen position at the $N_{\varepsilon 2}$ or $N_{\delta 1}$ atom of histidines [23]. The original crystallographic coordinates of the activation loop of the high pH GART structure (not passed through WHAT IF) were used for transfer in the low pH GART structure and subsequent unfolding. Then, the coordinates of the low pH GART structure were passed through WHAT IF for hydrogen addition and hydrogen bond network optimization. WHAT IF produced side chain flips for activation loop residues His121 and Asn127 in the high pH GART structure, but not in the low pH GART structure. Fragments of GART containing the activation helix were taken from the WHAT IF optimized whole structures of GART, by truncating the undesired coordinates.

3. Results

Fig. 1 shows a superposition of the two GART structures at high pH (3gar) and low pH (2gar). The enzyme is folded in both structures, with the exception of the activation loop-helix, which is fully unfolded at low pH but contains a helical segment at high pH. Note that the coordinates for the activation loop (residues 111–131) in the low pH GART structure (2gar) were disordered, thus

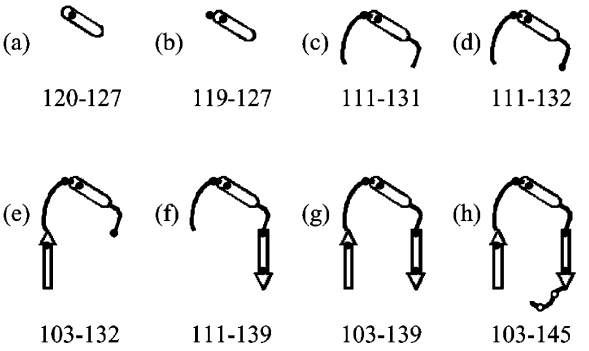

Fig. 4. The eight segments of the catalytic site (shown here at high pH) used in the calculations in addition to the whole protein. Solid circles indicate histidines, His108,119,121,132,137, and the open circles indicate Asp141 and Asp144.

absent from the crystallographic coordinates, and were modeled for our analysis as described in Methodology Section. Indeed, the missing coordinates of the activation loop were attributed to lack of electron density, which is characteristic of the high flexibility of this region [7]. We have focused our comparative study on the whole enzyme, as well as on eight segments of the region β5-activation loop-helix-β6-binding loop (Fig. 2), which forms the catalytic site of GART. Other differences in the region of interest of our study, involve the orientation of the binding loop, and the orientation of the side chains of His132 and His137 (Fig. 1) [7,8].

Fig. 4 shows the eight segments of GART structure we used in our step-wise calculations of stability of the activation loop-helix and super-secondary structure around it. Each segment contains the 8-residue region of the activation loop-helix of GART that undergoes the pH-dependent helix–coil transition.

Fig. 5(a–i) shows plots of the difference between apparent and model pK_a against residue number for the 8 structural segments (Fig. 4) and whole GART (Fig. 1). These plots depict the effect of structure on charge and the apparent pK_a values. They also help distinguish the particular ionizable residues that participate in, or are affected by, the step-wise structural changes we are introducing in our stability studies. Table 1

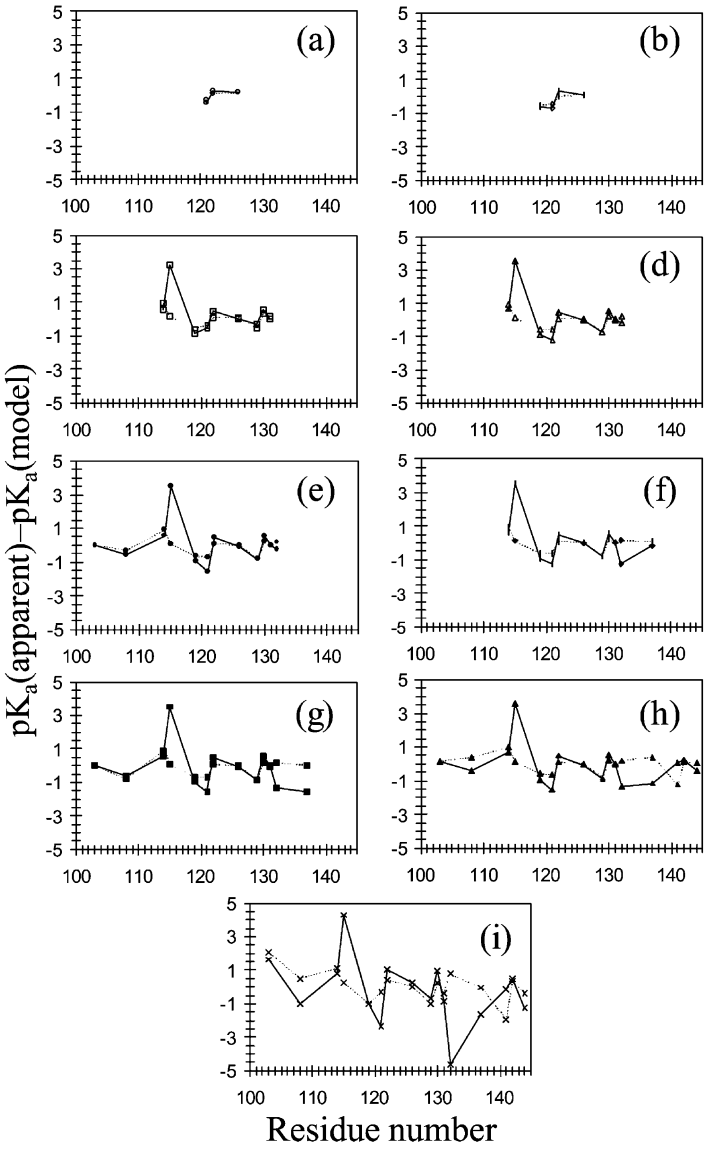

Fig. 5. Plots of difference of apparent and model pK_a against residue number for the helix state (solid line) and coil state (dashed line) for segment 120–127 (a), segment 119–127 (b), segment 111–131 (c), segment 111–132 (d), segment 103–132 (e), segment 111–139 (f), segment 103–139 (g), segment 103–145 (h), and segment 1–209 or whole enzyme (i). Only data for the region between residues 103 and 145 are plotted in the Panel (i) to facilitate comparison to Panels (a–h).

summarizes the apparent pK_a values for the 8 structural segments (Fig. 4) and whole GART (Fig. 1) for both the helix and coiled states.

Fig. 6 shows plots of the ionization free energy of unfolding, ΔG^{h-c}(pH), against pH for the whole GART and the eight GART segments of Fig. 4. Since both GART structures used in the calculation are in their native state and very similar to each other, ΔG^{h-c}(pH) corresponds mainly to structural differences in the activation loop-helix and other structural differences involving His132, His137 and the binding loop, when present, and

Table 1
Calculated apparent pK_a's of ionizable residues of the 8 GART segments of Fig. 4 and the whole GART enzyme, at high and low pH structures

Residue	pK_a (model)	Structural segment								
		pK_a (high pH)								
		120–127	119–127	111–131	111–132	103–132	111–139	103–139	103–145	1–209[a]
Arg103	12.0					12.0		12.0	12.1	13.6
His108	6.3					5.7		5.7	5.9	5.3
Lys114	10.4			11.0	11.0	11.0	11.0	11.0	11.1	11.2
Tyr115	9.6			12.9	13.1	13.1	13.1	13.1	13.2	13.9
His119	6.3		5.7	5.4	5.4	5.3	5.4	5.3	5.4	5.3
His121	6.3	5.8	5.6	5.8	5.1	4.7	5.1	4.8	4.8	3.9
Arg122	12.0	12.2	12.3	12.5	12.5	12.5	12.5	12.5	12.5	13.0
Glu126	4.4	4.6	4.5	4.4	4.4	4.3	4.4	4.3	4.3	4.6
Asp129	4.0			3.7	3.3	3.2	3.2	3.1	3.1	3.3
Glu130	4.4			5.0	4.9	4.9	5.0	5.0	5.0	5.4
Glu131	4.4			4.4	4.4	4.4	4.4	4.4	4.4	3.5
His132	6.3				6.1	6.1	5.0	4.9	5.0	1.7
His137	6.3						6.1	4.7	5.1	4.7
Asp141	4.0								4.0	3.8
Glu142	4.4								4.7	4.9
Asp144	4.0								3.6	2.7
	pK_a (model)	pK_a (low pH)								
Arg103	12.0					12.0		12.0	12.2	14.1
His108	6.3					6.0		5.5	6.7	6.8
Lys114	10.4			11.3	11.3	11.3	11.3	11.3	11.4	11.5
Tyr115	9.6			9.8	9.7	9.7	9.7	9.7	9.8	9.9
His119	6.3		5.8	5.7	5.7	5.6	5.7	5.6	5.7	5.3
His121	6.3	6.0	5.8	6.0	5.8	5.6	5.7	5.6	5.6	6.0
Arg122	12.0	12.1	12.0	12.1	12.1	12.1	12.1	12.1	12.1	12.4
Glu126	4.4	4.6	4.5	4.5	4.4	4.4	4.4	4.4	4.4	4.4
Asp129	4.0			3.5	3.3	3.2	3.2	3.2	3.2	3.0
Glu130	4.4			4.7	4.6	4.6	4.6	4.6	4.6	4.7
Glu131	4.4			4.6	4.5	4.4	4.4	4.3	4.4	4.1
His132	6.3				6.5	6.5	6.4	6.5	6.5	7.1
His137	6.3						6.4	6.3	6.7	6.3
Asp141	4.0								2.8	2.1
Glu142	4.4								4.5	4.8
Asp144	4.0								4.0	3.6

[a] From Ref. [8]. Only data of the catalytic site are shown here (region between residues 103–145) to facilitate comparison with the structural segments of Fig. 4.

their interactions. As ΔG^{h-c}(pH) increases the helical part of the activation loop-helix of GART is favored (Fig. 6), or, increase of ΔG^{h-c}(pH) in a given pH range corresponds to increase in the stability of the helical form. Our pH range starts at $pH_1 = 0$ [see Eq. (4)], where all curves cross zero. The maximum helical stability of each curve corresponding to the various GART segments of Fig. 4 is in the pH region 5.8–6.4 (or pH approximately 6; Fig. 6). Our study is comparative between low and high pHs.

The first segment (Fig. 4a) comprises residues 120–127, which are the part of the activation loop that is converted into an α-helix at high pH. This segment contains His121, which we have previously proposed to be responsible for the helix–

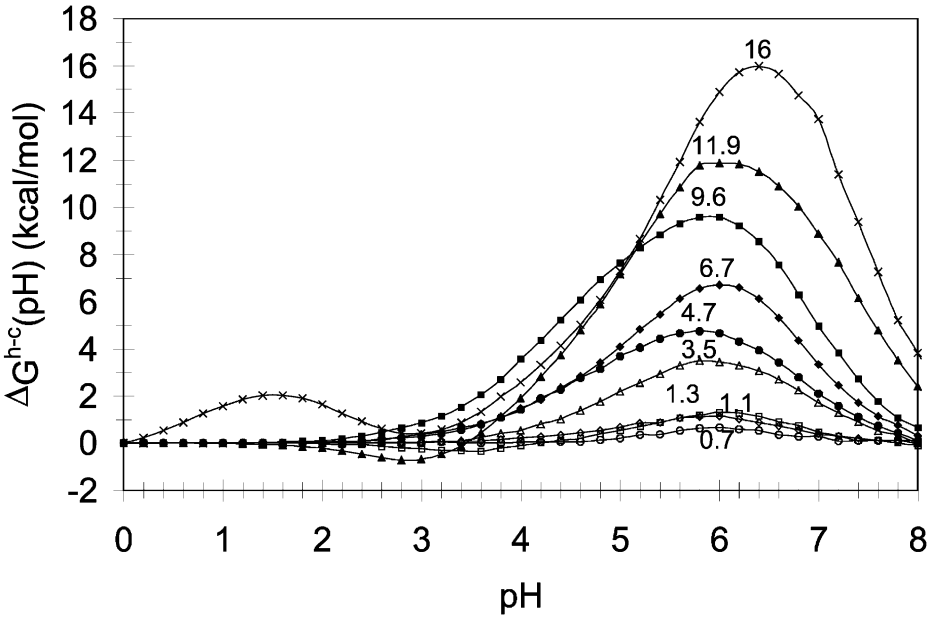

Fig. 6. Plots of ΔG^{h-c}(pH) against pH. Each plot shows the difference in ionization free energy at any pH minus the ionization free energy at pH 0, which is a common reference point for all plots. ΔG^{h-c}(pH) has been calculated for the eight segments of Fig. 4 and the whole enzyme (Fig. 1): segment 120–127 (open circles), segment 119–127 (open diamonds), segment 111–131 (open squares), segment 111–132 (open triangles), segment 103–132 (filled circles), segment 111–139 (filled diamonds), segment 103–139 (filled squares), segment 103–145 (filled triangles), and segment 1–209 or whole enzyme (×). At the top of each plot is shown the maximum value of ΔG^{h-c}(pH). The symbols of each plot correspond to the symbols of the plots of Panels (a–i) of Fig. 5 to facilitate comparison.

coil transition, depending on its protonation state [8]. It also contains Arg122 and Glu126, which we have previously proposed to participate in stabilization or destabilization of the activation helix. The corresponding curve (Fig. 6, open circles) shows an increase in ΔG^{h-c}(pH) by 0.7 kcal/mol. Given that the apparent pK_a values of His121, Arg122, do not show significant variation in the folded and unfolded structures of the activation helix (Fig. 5a), we attribute this slight increase in stability to the orientation of the ring of His121 (flipped by 180° in the helical form, see Methodology Section).

The second segment (Fig. 4b) adds a second histidine, His119, which we have also proposed to play a minor role in the stability of the activation helix of GART [8]. The change in the local charge distribution of the helical and coiled states owed to the addition of His119 is depicted in the apparent pK_a values of Fig. 5b. His119 is responsible for the small increase in the maximum value of ΔG^{h-c}(pH) from 0.7 kcal/mol to 1.1 kcal/mol (Fig. 6, open diamonds).

The third segment (Fig. 4c) adds the portion of the activation loop-helix, which remains a loop at both high and low pH. This segment comprises residues 111–119 at one end of the activation helix and residues 128–131 at the other end, and contains ionizable residues Lys114, Tyr115, Asp129, Glu130, and Glu131 (Fig. 2). The change in the local charge distribution of the helix and coil states because of the addition of these ionizable residues is depicted in the apparent pK_a values of Fig. 5c, with most prominent the contribution of Tyr115. The addition of these residues brings only a small change in the maximum ΔG^{h-c}(pH) from 0.7 kcal/mol to 1.3 kcal/mol (Fig. 6, open rectangles).

The fourth segment (Fig. 4d) adds a third histidine, His132, which we have previously

shown to strongly interact with His121 when the activation helix is present [8]. This strong interaction is demonstrated here in the apparent pK_a values of His121 and His132 (compare Fig. 5d and c). The addition of His132 on the activation loop-helix brings the maximum ΔG^{h-c}(pH) to 3.5 kcal/mol (Fig. 6, open triangles), which is a 2.2 kcal/mol increase compared to the third segment (without His132). This increase is of the order of a hydrogen bonding interaction.

The fifth segment (Fig. 4e) attaches the β-strand β5 on the amino terminus of the activation loop-helix, which contains a fourth histidine, His108, and Arg103. His108 is the catalytic histidine [2–5,7,8]. His108 is responsible for the difference in the local charge distribution of the helix and coil states (compare Fig. 5e and d). The addition of this strand brings the maximum ΔG^{h-c}(pH) to 4.7 kcal/mol (Fig. 6, filled circles), reflecting the added stability brought to the region by His108.

The sixth segment (Fig. 4f) attaches at the carboxy terminus of the activation loop-helix the remaining (in addition to His132) of β-strand β6, which contains a fifth histidine, the highly conserved His137. Addition of His137 radically alters the charge distribution of this segment, having a most prominent effect on His132 (compare Fig. 5f and Fig. 5d). Since His137 is distant to His132, this effect can be attributed to relay Coulombic interactions or desolvation. The addition of His137 brings the maximum ΔG^{h-c}(pH) to 6.7 kcal/mol (Fig. 6, filled diamonds), adding yet more stability to the region. We have previously shown that His137 participates in stabilizing the catalytic site by interacting with Asp144 and His108 [9].

The seventh segment (Fig. 4g) attaches strands β5 and β6 simultaneously at both ends of the activation loop-helix. The effect of the simultaneous presence of the two strands flanking the activation loop helix on the local charges is depicted in Fig. 5g and has significant impact on His137 (compare Fig. 5g and Fig. 5f). The combined effect of strands β5 and β6 accounts for the increase of the maximum ΔG^{h-c}(pH) to 9.6 kcal/mol (Fig. 6, filled rectangles).

The eighth segment (Fig. 4h) attaches the binding loop, comprising residues 140–145, which contains the catalytic Asp144 [2–5,7,9] and other ionizable residues Asp141 and Glu142. When substrate and cofactor are bound to GART, Asp144 stabilizes substrate GAR and catalytic histidine His108. Fig. 5h shows how the local charge rearrangements significantly affect the pK_a value of His108 (compare Fig. 5h and g). The local charge changes are attributed to the presence of Asp141 and Asp144 whose pK_a values show sizeable differences at high and low pHs (Table 1). This segment brings the maximum ΔG^{h-c}(pH) to 11.9 kcal/mol (Fig. 6, filled triangles). The addition of the binding loop completes the formation of the catalytic site.

Finally, when adding to the catalytic site the remaining of the enzyme we observe a large effect in the charge distribution of the catalytic site (compare Fig. 5i and h). There are large shifts in the pK_a values of His108, His121 and His132 from their model pK_a values (with most prominent that of His132), when comparing the activation helix and coil states of the enzyme (Table 1). The addition of the remaining enzyme around the catalytic site brings an increase in the maximum ΔG^{h-c}(pH) by only 4.1 kcal/mol to a value of 16 kcal/mol (Fig. 6, × symbols). This corresponds to the ionization free energy of the whole GART between low and high pH.

The ionization free energy ΔG^{h-c}(pH) of all segments of Fig. 4 increases as we move from pH 0 to pH approximately 6, demonstrating maximum stabilization of the helical segment at pH approximately 6. Also, stepwise addition of structure that flanks the activation helix [segment (a) of Fig. 4] results in variable increase of the ionization free energy ΔG^{h-c}(pH), providing a measure of the degree of stabilization introduced by the additional structure.

4. Discussion

The experimentally observed pH-dependence of the helix–coil transition of the activation loop-helix of GART suggested the importance of electrostatics in the helix formation and stability. Our goal was to elucidate the minimal structural contributions and the most significant electrostatic interactions responsible for the stability of the

activation helix, the catalytic site, and the whole GART enzyme. The present analysis is a continuation of our previous work of pK_a calculations and electrostatic modeling of GART [8,9]. We have performed electrostatic calculations using available crystallographic structures with additional modeling of coordinates, when necessary, to predict the mean net charges of GART and several GART segments that contain the activation helix. The mean net charges were used afterwards to estimate the free energy of the activation helix–coil transition, ΔG^{h-c}(pH), which is a quantity associated with stability of the activation helix. The free energy ΔG^{h-c}(pH) is equivalent to ionization free energy of the helix–coil transition, $\Delta\Delta G^{c,h,\mathrm{ion}}$(pH) [Fig. 3 and Eqs. (7) and (8)] when calculated relatively to a reference pH value, pH_1, which is taken to be equal to zero in our calculations. Our comparison focuses on: (1) evaluation of the relative stability of the activation helix of GART at high and low pHs and (2) evaluation of the step-wise increase of stability of the activation helix of GART with the step-wise addition of secondary structure surrounding the activation helix. More specifically, in (1) our comparison is made when going from pH 0 to at pH approximately 6, which is the pH of maximum stability. This comparison is made 9 times within each of the 8 GART segments of Fig. 4 and the whole GART (Fig. 1). In (2) we compare the step-wise increase of the maximum stability of the activation helix of GART when going from segment 1 to segment 8 and whole GART. An intermediate result of our calculations is the prediction of apparent pK_a values for ionizable residues (Table 1). Apparent pK_a are comprehensible indicators of the combination of desolvation and pair-wise and multiple Coulombic interactions that contribute to the stability of the activation helix of GART and influence the experimentally observed pH-dependent helix–coil transition.

We have shown that the increase of pH from 0 to approximately 6 produces an increase in the stability of the activation helix alone by 0.7 kcal/mol. Addition of His119, His132, His108, His137 and Asp141 with Asp144, together with the structures associated with them, amplifies the stability of the activation loop-helix and surrounding structure by 0.4, 2.2, 1.2, 3.2 and 2.3 kcal/mol, respectively, [these are differences of the maximum ΔG^{h-c}(pH) values in corresponding curves of Fig. 6]. Finally, addition of the remaining of the enzyme produces further increase in stability by 4.1 kcal/mol, reflecting contributions from sites away from the active site. All these contributions show an overall higher stability by 11.9 kcal/mol for the active site and by 16 kcal/mol for the whole enzyme at pH approximately 6 compared to pH 0. These changes in ionization free energy are due to the combined electrostatic effects of desolvation and Coulombic interactions with electric dipoles and other ionizable sites in their ionized form.

The 2.2 kcal/mol increase of the stability of the activation loop-helix upon addition of His132 is indicative of the strong interaction between His121 and His132 and is of the order of the stability of a hydrogen bond [26,27]. In our earlier calculations of apparent pK_a values of ionizable residues of GART, we showed that His121 and His132 are favored to be protonated (charged) at low pH, with pK_a's of 6.0 and 7.1, respectively, and neutral at high pH, with pK_a's of 3.9 and 1.7, respectively, (Table 1) [8]. At high pH, when we theoretically mutated His132, the pK_a of His121 jumped from 3.9 to 6.3 and when we theoretically mutated His121, the pK_a of His132 jumped from 1.7 to 3.5 [8]. These results were the basis of our hypothesis that His121 forms a molecular switch for the helix-coil transition of the activation helix, depending on its protonation state. When His121 is neutral the activation helix is formed; and when His121 is charged, the activation helix is unwound. In addition, we proposed that the strong electrostatic interaction of His121–His132 could act as a stabilizer or destabilizer of the activation helix, depending on their protonation states and relative orientation of their rings. If His121 is the switch that turns on the formation of the activation helix and shields the catalytic site from solvent, His132 plays the role of locking or unlocking the activation helix onto the catalytic site at high pH. Conversely, at low pH, His121 switches off the helix as His132 releases it from the catalytic site.

It is evident that the relative stability of the whole enzyme of GART between the pHs of the two crystallographic structures we used (pH 7.5

and 3.5) is dominated by the stability of the catalytic site, as there is only a 4.1 kcal/mol increase in stability when the rest of the enzyme is added to the catalytic site (Fig. 6). According to our calculations, the pH of maximum stability for the whole GART is 6.4 (Fig. 6). Likewise, the pH of maximum stability for the GART segments that contain the activation helix of GART is in the range of 5.8–6.0. Interestingly, in native GART the maximal catalytic rate occurs at pH approximately 8 [4], where the activation helix should be destabilized compared to pH 6.4 according to our calculations (Fig. 6). It may be possible that this destabilization is important for substrate/cofactor entry and exit into the catalytic site.

We do not have a direct evidence for the pH where the helix–coil transition occurs in solution. The two crystallographic structures we used in our calculations were determined at pH 3.5 and 7.5, which places the helix–coil transition between these two pHs. We know that crystallographic structures of native substrate bound GART with formed activation helix, have been determined at pHs 7.5 and 7.4 [2,5,28]. We also know that crystallographic structures of native GART (inhibitor bound or free) with unwound activation helix, have been determined at pHs 6.75 and 6.3 [5,29,30]. It is not clear if these reported pHs are of the mother liquor used for crystal growth or they represent the actual pH of the crystals. (Protein self-buffering effects at high protein concentrations are well known.) Another complication at these pHs arises because GART is also found in dimeric form at $pH < 7$ [5,6,29,30]. This does not allow for direct comparison with the E70A GART, used in our calculations, which is monomeric at all pHs [7,31]. The E70A mutation, which is responsible for loss of dimerization at low pH (Glu70 is located at the dimer interface), is remote to the activation loop-helix and catalytic site. We do not have an experimental indication that the E70A mutation will affect the pH where the helix–coil transition occurs. In addition, the high pH crystallographic structures of E70A GART and substrate/pseudocofactor-bound native GART are very similar with the exception of the orientation of the binding loop [2,5,7,28]. Based on our calculations the activation helix of GART should be well stabilized at pH 6.4 with the helix–coil transition occurring at a lower pH (approx. 5.4) represented by the inflection point the corresponding curve in Fig. 6. Experimental data that measure the degree of helicity (e.g. using circular dichroism) in the pH range 0–8 are needed for a meaningful comparison with our calculations. Such data will also demonstrate if the activation helix unwinds again at higher pH. This is suggested by the plots of Fig. 6 where the stabilities at pH approximately 3 and approximately 8 are similar and significantly decreased compared to pH approximately 6. It may also be possible that binding of the cofactor and substrate helps to further stabilize the activation helix at high pH. This would be consistent with crystallographic and binding kinetic data of native GART [2,4,5].

In the current study we have evaluated in terms of stability the complex electrostatic coupling of the activation loop-helix, surrounding strands β5 and β6, and the binding loop, which form the catalytic site. There is a network of electrostatic interactions that involves five histidines, His108, His119, His121, His132, His137, and two aspartic acids, Asp141, Asp144. If the sequence of the activation helix and the ionization state of His121 are important for secondary structure specificity, the electrostatic interaction of His121–His132 and the other ionizable residues in the vicinity are important for helix stabilization or destabilization. Also, the His121–His132 interaction is important for side chain conformational specificity. Additional non-polar (cavity–van der Waals) desolvation effects and configurational entropic effects are also expected to contribute to the stability of the activation helix. Availability of experimental folding data will be necessary to evaluate the magnitude of these effects and their contributions to stability.

Acknowledgments

This work was supported by NIH grants GM19879 (DM), GM54038 (PAJ), and grants from NIH, NSF, SDSC (JAM). We thank Drs Gert Vriend and Jens Nielsen for providing us with WHAT IF.

References

[1] R.H. Garrett, C.M. Grishnan, Biochemistry, Saunders College Publishing, Harcourt Brace College Publishers, USA, 1985.

[2] S.E. Greasley, M.M. Yamashita, H. Cai, S.J. Benkovic, D.L. Boger, I.A. Wilson, New insights into inhibitor design from the crystal structure and NMR studies of *Escherichia coli* GAR transformylase in complex with beta-GAR and 10-formyl-5,8,10-trideazafolic acid, Biochemistry 38 (1999) 16783–16793.

[3] J.H. Shim, S.J. Benkovic, Evaluation of the kinetic mechanism of Escherichia coli glycinamide ribonucleotide transformylase, Biochemistry 37 (1998) 8776–8782.

[4] J.H. Shim, S.J. Benkovic, Catalytic mechanism of *Escherichia coli* glycinamide ribonucleotide transformylase probed by site-directed mutagenesis and pH-dependent studies, Biochemistry 38 (1999) 10024–10031.

[5] R.J. Almassy, C.A. Janson, C.C. Kan, Z. Hostomska, Structures of apo and complexed *Escherichia coli* glycinamide ribonucleotide transformylase, Proc. Natl. Acad. Sci. USA 89 (1992) 6114–6118.

[6] C.A. Mullen, P.A. Jennings, Glycinamide ribonucleotide transformylase undergoes pH-dependent dimerization, J. Mol. Biol. 262 (1996) 746–755.

[7] Y. Su, M.M. Yamashita, S.E. Greasley, C.A. Mullen, J.H. Shim, P.A. Jennings, A pH-dependent stabilization of an active site loop observed from low and high pH crystal structures of mutant monomeric glycinamide ribonucleotide transformylase at 1.8 to 1.9 A, J. Mol. Biol. 281 (1998) 485–499.

[8] D. Morikis, A.H. Elcock, P.A. Jennings, J.A. McCammon, Native-state conformational dynamics of GART: a regulatory pH-dependent coil-helix transition examined by electrostatic calculations, Protein Sci. 10 (2001) 2363–2378.

[9] D. Morikis, A.H. Elcock, P.A. Jennings, J.A. McCammon, Proton transfer dynamics of GART: the pH-dependent catalytic mechanism examined by electrostatic calculations, Protein Sci. 10 (2001) 2379–2392.

[10] A.S. Yang, B. Honig, On the pH dependence of protein stability, J. Mol. Biol. 231 (1993) 459–474.

[11] A.S. Yang, B. Honig, Structural origins of pH and ionic strength effects on protein stability. acid denaturation of sperm whale apomyoglobin, J. Mol. Biol. 237 (1994) 602–614.

[12] J. Antosiewicz, J.A. McCammon, M.K. Gilson, Prediction of pH-dependent properties of proteins, J. Mol. Biol. 238 (1994) 415–436.

[13] Y.N. Vorobjev, H.A. Scheraga, B. Honig, Theoretical modeling of electrostatic effects of titratable side-chain groups on protein conformation in a polar ionic solution. 2 pH-induced helix-coil transition of poly(L-lysine) in water and methanol ionic solutions, J. of Phys. Chem. 99 (1995) 7180–7187.

[14] A.H. Elcock, Realistic modeling of the denatured states of proteins allows accurate calculations of the pH dependence of protein stability, J. Mol. Biol. 294 (1999) 1051–1062.

[15] C. Tanford, Protein denaturation. C. theoretical models for the mechanism of denaturation, Adv. Protein Chem. 24 (1970) 1–95.

[16] M.K. Gilson, Multiple-site titration and molecular modelling: two rapid methods for computing energies and forces for ionizable groups in proteins, Proteins Struct. Funct. Genet. 15 (1993) 266–282.

[17] J. Antosiewicz, J.A. McCammon, M.K. Gilson, The determinants of pK_a's in proteins, Biochemistry 35 (1996) 7819–7833.

[18] J.D. Madura, M.E. Davis, M.K. Gilson, R.C. Wade, B.A. Luty, J.A. McCammon, Biological applications of electrostatic calculations and brownian dynamics simulations, Rev. Comput. Chem. 5 (1994) 229–267.

[19] J.D. Madura, J.M. Briggs, R.C. Wade, M.E. Davis, B.A. Luty, A. Ilin, J. Antosiewicz, M.K. Gilson, B. Bagheri, L.R. Scott, J.A. McCammon, Electrostatics and diffusion of molecules in solution: simulations with the University of Houston Brownian Dynamics Program, Comput. Phys. Commun. 91 (1995) 57–95.

[20] D. Sitkoff, K.A. Sharp, B. Honig, Accurate calculation of hydration free energies using macroscopic solvent models, J. Phys. Chem. 98 (1994) 1978–1988.

[21] A.D. MacKerell, J. Wiórkiewicz-Kuczera, K. M, CHARMM22 Parameter Set, Department of Chemistry, Harvard University, Cambridge, MA, 1995.

[22] B.R. Brooks, R.E. Bruccoleri, B.D. Olafson, D.J. States, S. Swaminathan, M. Karplus, CHARMM: a program for macromolecular energy, minimization and dynamics calculations, J. Comput. Chem. 4 (1983) 187–217.

[23] J.E. Nielsen, K.V. Andersen, B. Honig, R.W. Hooft, G. Klebe, G. Vriend, Improving macromolecular electrostatics calculations, Protein Eng. 12 (1999) 657–662.

[24] G. Vriend, WHAT IF: a molecular modeling and drug design program, J. Mol. Graph. 8 (1990) 52–56, 29.

[25] R.W.W Hooft, C. Sander, G. Vriend: Positioning hydrogen atoms by optimizing hydrogen-bond networks in protein structures. Proteins: Struct. Funct. Genet. 26 (1996).

[26] T.E. Creighton, Proteins: Structures Molecular Properties, W.H. Freeman and Company, New York, 1997.

[27] N. Ben-Tal, D. Sitkoff, I.A. Topol, A.S. Yang, S.K. Burt, B. Honig, Free energy of amide hydrogen bond formation in vacuum, in water, and in liquid alkane solution, J. Phys. Chem. 101 (1997) 450–457.

[28] S.E. Greasley, T.H. Marsilje, H. Cai, S. Baker, S.J. Benkovic, D.L. Boger, Unexpected formation of an epoxide-derived multisubstrate adduct inhibitor on the active site of GAR transformylase, Biochemistry 40 (2001) 13538–13547.

[29] P. Chen, U. Schulze-Gahmen, E.A. Stura, J. Inglese, D.L. Johnson, A. Marolewski, Crystal structure of glycinamide ribonucleotide transformylase from *Escherichia coli* at 3.0 a resolution a target enzyme for chemotherapy, J. Mol. Biol. 227 (1992) 283–292.

[30] C. Klein, P. Chen, J.H. Arevalo, E.A. Stura, A. Marolewski, M.S. Warren, Towards structure-based drug design: crystal structure of a multisubstrate adduct complex of glycinamide ribonucleotide transformylase at 1.96 A resolution, J. Mol. Biol. 249 (1995) 153–175.

[31] C.A. Mullen, P.A. Jennings, A single mutation disrupts the pH-dependent dimerization of glycinamide ribonucleotide transformylase, J. Mol. Biol. 276 (1998) 819–827.

[32] N. Guex, M.C. Peitsch, SWISS-MODEL and the Swiss-PdbViewer: an environment for comparative protein modeling, Electrophoresis 18 (1997) 2714–2723.